

> REPLACE THIS LINE WITH YOUR PAPER IDENTIFICATION NUMBER (DOUBLE-CLICK HERE TO EDIT) <

1

# Multi-Beam 3D Printed Luneburg Lens Fed by Magneto-Electric Dipole Antennas for Millimeter-Wave MIMO Applications

Yujian Li, *Member, IEEE*, Lei Ge, *Member, IEEE*, Meie Chen, Zhan Zhang, Zheng Li, *Member, IEEE*, and Junhong Wang, *Senior Member, IEEE*

**Abstract**—A 3D printed Luneburg lens with a novel simplified geometry is presented. Rod-type structures are employed as the unit cell of the gradient-index material to realize the required permittivity distribution in the lens. A prototype designed in Ka-band is manufactured successfully by using a commercial 3D printing facility. The substrate integrated waveguide (SIW) fed magneto-electric (ME) dipole antenna with end-fire radiation is introduced as the feed of the Luneburg lens due to its wideband performance and compact configuration. By combining the lens with a set of the ME-dipoles, a millimeter-wave (mm-wave) multi-beam Luneburg lens antenna is designed, fabricated and measured. An overlapped impedance bandwidth of wider than 40% that can cover the entire Ka-band and mutual coupling below -17 dB are verified by the fabricated prototype. Nine stable radiation beams with a scanning range between  $\pm 61^\circ$ , gain up to 21.2 dBi with a variation of 2.6 dB and radiation efficiency of around 75% are achieved as well. With advantages of good operating features, low fabrication costs and ease of integration, the proposed multi-beam Luneburg lens antenna would be an promising candidate for the fifth-generation (5G) mm-wave multiple-input multiple-output (MIMO) applications in 28 and 38 GHz bands.

**Index Terms**—Luneburg lens, multi-beam antenna, 3D printing, the fifth-generation (5G) communications, millimeter-waves.

## I. INTRODUCTION

Millimeter-wave (mm-wave) multiple-input multiple-output (MIMO) with the ability to enhance the data rate significantly has been considered as one of the key technologies for the fifth-generation (5G) mobile communications [1]. However, the implementation of the mm-wave MIMO in practice is still a stiff task and thus has received increasing attention recently. One of the key challenges is the realization of the antenna that can generate a large number of radiation beams. According to the requirement of the fully-digital beamforming technology, the number of radio-frequency (RF) chains used in the system is equal to that of the radiating elements composing the antenna array, which results in unaffordable hardware cost and power consumption for a large-scale mm-wave array [2]. In order to reduce the

Manuscript received by \*, 2018. This work was supported in part by the National Natural Science Foundation of China under Grant No. 61822103 and the National Nature Science Foundation of China under Grant 61671052.

Y. J. Li, M. E. Chen, Z. Zhang, Z. Li and J. H. Wang are with the Institute of Lightwave Technology, Beijing Jiaotong University, Beijing 100044, China (e-mail: liyujian@bjtu.edu.cn). L. Ge is with the College of Electronic Science and Technology, Shenzhen University, Shenzhen, China. (e-mail: leige@szu.edu.cn).

required RF chains, the hybrid beamforming technique combining analog and digital processing methods has been investigated in the literature [3]. Reported studies revealed that the multi-beam lens antenna with convenience of fabrication, high efficiency and low costs would be a promising solution to realize the analog beamforming for mm-wave MIMO applications [4]–[5]. In comparison with the planar or extended hemispherical lens structure [6]–[7], the spherical lens [8]–[9] enables to radiate beams scanning in a wide angular range without performance degradation. Hence, it would be desirable for mobile communications.

As a type of the spherical lens antenna, the Luneburg lens initially invented in [10] has been persistently investigated for decades [11]. Different from the spherical lens with a constant index, the permittivity of the material constructing an ideal Luneburg lens continuously varies as a function of the lens radius, which is difficult to fulfill in practice. As a result, various design methodologies to simplify the lens geometry have been studied. The layered approach where the entire Luneburg lens is divided into a series of shells is the most used method [12]–[14]. Promising results can be obtained, but the shells with different permittivities increase the fabrication complexity and costs significantly. The sliced Luneburg lens consisting of a set of stacked gradient-index material slabs has also been reported [15]–[16]. The varying permittivity can be achieved by tuning the size of the periodic holes drilled in the slabs. The type of the materials used in lens design is reduced, but the perforation process is still time consuming and a higher accuracy is needed with the increase of frequency, which inevitably restricts the feasibility of this method at mm-waves.

In recent years, three-dimensional (3D) printing, or named as additive manufacturing, has offered a new way to implement complex 3D structures with low costs. As one of the dielectric 3D printing techniques, the polymer jetting is suitable for mm-wave device design because of its good printing resolution [17]. Some mm-wave and Terahertz (THz) reflect arrays and lenses with solid structures have been realized successfully by adopting the polymer jetting [18]–[19]. For non-uniform geometries such as the Luneburg lens, the concept of the gradient-index material can be applied in 3D printing conveniently. By employing the cubical lattice as the unit cell of the gradient-index material, a Luneburg lens based on the Gutman's solution was printed first in Ka-band [20]. However, due to the use of ceramic polycrystalline with a high permittivity as printed material, the required low index cannot be reached by the cubical lattice, which degrades its bandwidth and radiating features. More recently, a 3D printed Luneburg

&gt; REPLACE THIS LINE WITH YOUR PAPER IDENTIFICATION NUMBER (DOUBLE-CLICK HERE TO EDIT) &lt;

2

lens with wide bandwidth and stable radiation performance was presented in 10-GHz band [21]. The combination of a large number of dielectric blocks and a rod space frame was used for building the gradient-index material. However, as the dimension of the rod space frame is much smaller comparing with the operating wavelength, this structure would become quite weak at mm-waves when support material is removed, which is not acceptable in practice. Meanwhile, the complicated spacing in the frame also increases the difficulty of removing the support material. Assembling the components printed separately may be a method to solve the issues, but obviously it sacrifices the benefit of the direct manufacturing. Therefore, it is seen that investigation on simplified geometry without tiny structures is of significant importance to the mm-wave 3D printed Luneburg lens.

Theoretically, the collimating properties of the Luneburg lens is irrespective of diameter [11]. In practice, however, this also depends on the illumination from the feed structure. Hence, for the purpose of designing a multi-beam Luneburg lens antenna, the feeding structure plays a crucial role as well. The bandwidth and radiation characteristics of the feed affect the lens performance directly. Moreover, the minimum crossover level between radiating beams is determined by the volume of feeding elements. Wideband open-ended waveguides [13], [15]-[16], [20]-[21] and horn antennas [22] are widely used for the Luneburg lens with a single feed, but they are not easy to accomplish the multi-beam radiation with a small crossover level due to the bulky geometries. The microstrip antenna [23], monopole antenna [17] and log periodic dipole antenna [24] can be used in multi-beam Luneburg lens designs. Unfortunately, their relatively narrow bandwidths or unstable radiation features would restrict the achievable performance of the lens. As a kind of the complementary source antenna, the magneto-electric (ME) dipole originally reported in [25] has a wide operating band and excellent radiation properties. Recently, substrate integrated ME-dipoles with compact geometries have also been studied in mm-wave bands [26]-[27]. However, up to now there is no reported work regarding the use of ME-dipole antennas as the feed of the multi-beam Luneburg lens according to the best of the authors' knowledge.

Based on rotational symmetry of the spherical lens, a Luneburg lens with a novel simplified geometry is presented in this paper. Different from the reported 3D printed Luneburg lenses, the rod-type structure is adopted to compose the required gradient-index material. Benefiting from the material without very fine details and with a lower achievable effective permittivity, the Luneburg lens designed in Ka-band can be fabricated conveniently by using commercial 3D printing technology. On the other hand, the substrate integrated waveguide (SIW) fed ME-dipole antennas with end-fire radiation originally reported in [28] are introduced as the feed array of the lens. It is found that better radiation properties can be achieved in comparison with the traditional waveguide or dipole feed. Because of the wide operating band covering the whole Ka-band, stable multi-beam radiation performance, low fabrication cost and ease of integration with circuit systems, the proposed multi-beam 3D-printed Luneburg lens antenna would be attractive for mm-wave MIMO applications in 5G mobile communications.

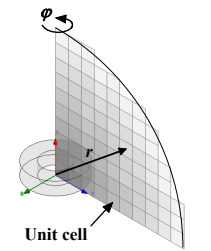


Fig. 1. Geometry simplification of the Luneburg lens.

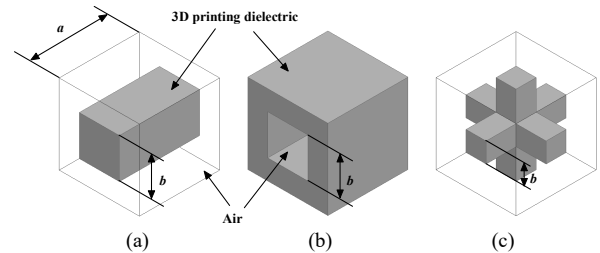


Fig. 2. Cubes for evaluating the effective dielectric constant of the gradient-index material. (a) dielectric rod (Type A), (b) dielectric hole (Type B), (c) dielectric lattice (Type C).

The paper is organized as follows. Section II describes the design method of the 3D printed Luneburg lens. The multi-beam lens antenna performance is analyzed in detail in Section III. Experimental results are illustrated in Section IV and a brief conclusion is finally given in Section V.

## II. DESIGN OF THE 3D PRINTED LUNEBURG LENS

### A. Geometry Simplification

Although the dielectric constant of the material varying along the radius direction, the Luneburg lens is still a spherical structure with rotational symmetry. By employing this feature, the lens in this work can be designed on a quarter of the spherical sectional plane first as illustrated in Fig. 1. The considered plane is then divided into a series of square cells. The required permittivity value in each cell can be obtained by calculating the distance  $r$  between the core of the lens and the center of the cell as shown in Fig. 1. By rotating all the square cells around  $z$ -axis, a series of dielectric rings are generated as indicated in Fig. 1, which can construct the Luneburg lens. In order to realize the varied dielectric constant in these ring structures, the 3D printed gradient-index material with a uniform geometry in  $\phi$  direction is applied in this work. Compared with the cubical lattice topology utilized in [20] and [21], the proposed topology with rotational symmetry are helpful to further simplify the 3D printed Luneburg lens but not introducing undesirable small dimensions.

### B. Gradient-Index Material Design

In reported studies, the 3D printed gradient-index material consists of a kind of printing material and the air [20], [21]. Therefore, the achievable highest and lowest effective dielectric constant of the gradient-index material are determined by the dielectric constant of the printing material and the minimum printable dimension. Moreover, the unit cell constructing the material should be small enough in

&gt; REPLACE THIS LINE WITH YOUR PAPER IDENTIFICATION NUMBER (DOUBLE-CLICK HERE TO EDIT) &lt;

3

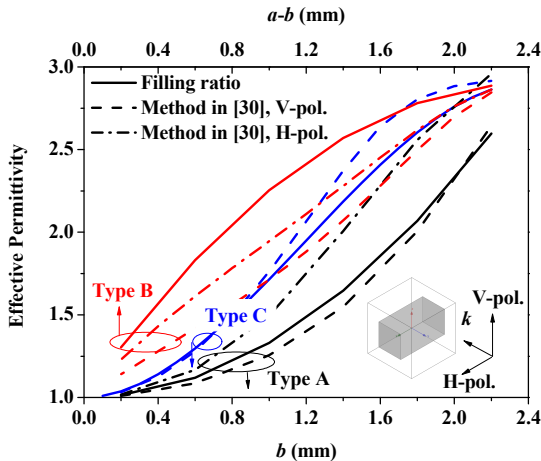


Fig. 3. Effective permittivity of the three types of materials as a function of the geometry parameter.

comparison with the operating wavelength. The dielectric constant of the available polymer-based 3D printing materials is usually close to 3 or even higher, while the material with a variable dielectric constant between 1 and 2 is needed for the Luneburg lens design [10]. As a result, it is found that restricted by the minimum printable dimension and the relatively high dielectric constant of the available printing materials, the effective dielectric constant close to 1 is not easy to realize at mm-wave frequencies based on the reported gradient-index material structures.

Actually, variation in the unit cell geometry of the gradient-index material can provide additional degree of freedom to widen the tuning range of the effective dielectric constant without need of changing the printing material and fabrication constraints, which can be utilized to overcome the aforementioned issues. Unfortunately, this has been seldom addressed in the literature up to now. Three types of the material with different unit cell structures are considered here as shown in Fig. 2. For the purpose of convenience to evaluate the effective dielectric constant of the gradient-index material, a cube unit cell with a length of  $a$  is cut from the ring structures with a sectional dimension of  $a \times a$ . A solid rod with a side length of  $b$  and a cube drilled a hole with a side length of  $b$  as well are assigned as cells Types A and B separately. Type B is similar to the gradient-index material employed by the sliced Luneburg lens designs in [15] and [16]. Additionally, the cubical lattice with a side length  $b$  which has been adopted in [20] and [21] is Type C as shown in Fig. 2. Photopolymer VeroClear [19] is used as the 3-D printer material due to its relatively low dielectric constant of 2.9 and loss tangent of 0.01 at mm-wave frequencies [18]. The side length  $a$  is fixed to 2.4 mm to guarantee a small cube size. The polymer jetting method is employed to print the proposed design. The resolution and the fabrication tolerance of the used 3D printer are about 0.04 mm and 0.1 mm, respectively.

Two kinds of methods are employed here to obtain the effective dielectric constants of the three types of gradient-index materials. The first one is based on the filling ratio  $R$  of the printer material [21]. A general formula for the effective dielectric constant calculation can be given by

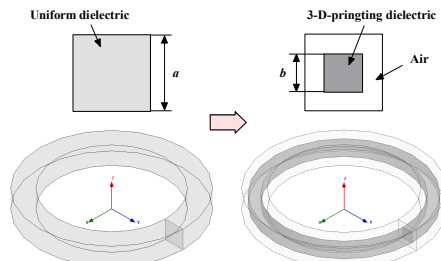


Fig. 4. Geometry of the dielectric ring structure composing the Luneburg lens.

TABLE I  
DIMENSIONS OF THE DIELECTRIC RINGS

Type index	1	2	3	4	5
$b$ (mm)	1.74	1.72	1.69	1.63	1.56
Type index	6	7	8	9	10
$b$ (mm)	1.45	1.32	1.15	0.92	0.55

$$\varepsilon_{re} = \varepsilon_r \times R + (1 - R) \quad (1)$$

where  $R$  is the ratio of the volume of the printer material to that of the cube. By this mean, the effective dielectric constant of the material can be determined approximately without the consideration on the specific features of the incident wave. However, as the cube structure in horizontal plane is different with that in vertical plane, the polarization characteristics of the gradient-index material Type A and Type B would be analyzed. To this end, the second method based on the S-parameters is applied. The cube structure accompanied with the periodic boundaries is simulated with the help of a commercial full-wave electromagnetic solver Ansys HFSS [29]. The incident waves with the vertical and horizontal polarizations as indicated in Fig. 3 are set in simulation, respectively. Then the effective dielectric constant of the material can be extracted from the S-parameters [30]. The results achieved in Fig. 3 as a function of the thickness of the printed material. It can be seen in Fig. 2 that the thickness is the side length  $b$  for Types A and C, while is  $a-b$  for Type B. Besides, it is noted that for the material Type C, only the vertically polarized incident wave is considered in simulation due to its identical geometry features in the two orthogonal planes.

For all the three kinds of materials,  $\varepsilon_{re}$  is close to 1 when  $R$  approaches 0, and is close to 2.9 when  $R$  approaches 1. However, remarkable discrepancy can be observed between the three curves of  $\varepsilon_{re}$  shown in Fig. 3, which verifies the effect of the unit cell structure on the effective dielectric constant. Generally, for the printing material with a fixed thickness, a relatively low  $\varepsilon_{re}$  can be achieved by Type A in comparison with Types B and C. According to the fabrication experience, the minimum robust thickness is around 0.6 mm for VeroClear material in 3D printing process. Therefore, the reachable lowest effective dielectric constant for Types B and C is not less than 1.3, which is not easy to meet the requirement for Luneburg lens design. On the other hand, the effective dielectric constant approaching 1 can be achieved by the material Type A, which making the realization of a mm-wave 3D printed Luneburg lens possible under the same constraints.

&gt; REPLACE THIS LINE WITH YOUR PAPER IDENTIFICATION NUMBER (DOUBLE-CLICK HERE TO EDIT) &lt;

4

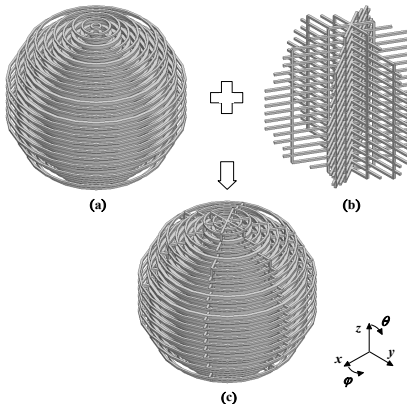


Fig. 5. Geometry of the proposed 3D printed Luneburg lens. (a) lens without the connecting frame, (b) connecting frame, (c) lens with the connecting frame.

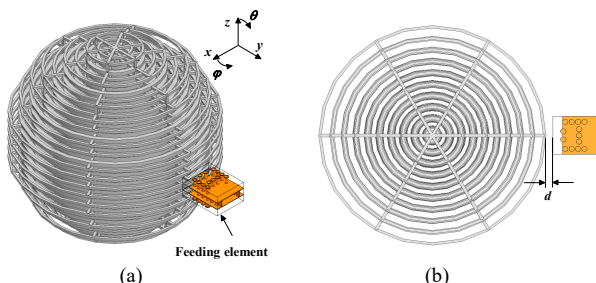


Fig. 6. Geometry of the 3D-printed Luneburg lens with a single feed. (a) Perspective view, (b) top view.

As shown in Fig. 3, the effective dielectric constants of the material Types A and B vary with the polarization of the incident wave, which confirms that they are anisotropic materials due to the asymmetrical geometry. For the material Type A, the curve of the effective permittivity for the vertically polarized incident wave agrees well with that calculated from the filling ratio, but is lower than the counterpart for the horizontally polarized incident wave. In this work, the 3-D printed Luneburg lens is designed with a vertically polarized feed.

### C. Lens Geometry

The geometry of a dielectric ring consisting of the cell Type A is given in Fig. 4. The value of  $b$  can be determined from the results shown in Fig. 3 for a required effective permittivity. In this design, ten columns of the square cells in  $y$ -direction are used for filling the sectional plane as indicated in Fig. 1. The values of  $b$  for all unit cells are classified into ten types based on the distance  $r$ . Detailed values are listed in Table I. Fig. 5 presents the final geometry of the proposed 3D printed Luneburg lens composed of the dielectric rings. Three sets of connecting frames with a width of 0.6 mm are added to combine all the rings together. It should be noted that the frames do not affect the radiation performance of the lens significantly since they only exist in three vertical planes.

## III. DESIGN OF THE MULTI-BEAM LENS ANTENNA

The multi-beam antenna is proposed in this section by employing the 3D-printed Luneburg lens investigated in

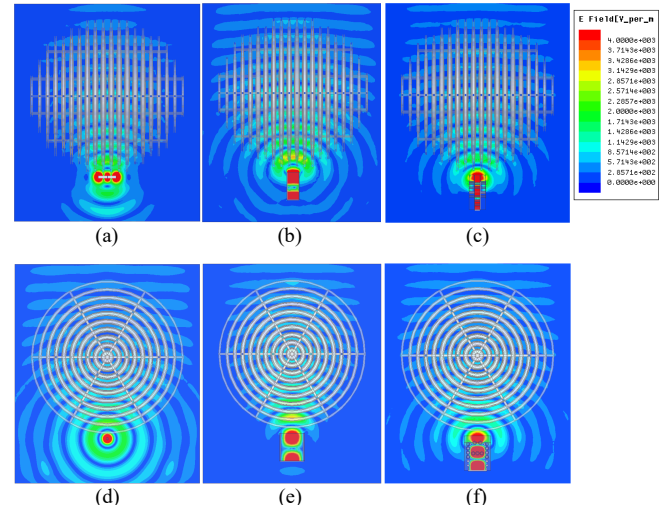


Fig. 7. Simulated electric field distributions across the lens with different feeds. (a) E-plane, electric dipole, (b) E-plane, open-ended waveguide, (c) E-plane, ME-dipole, (d) H-plane, electric dipole, (e) H-plane, open-ended waveguide, (f) H-plane, ME-dipole.

Section II. The effect of a feeding structure on radiation properties of the lens, and the performance of the lens fed by a single antenna and multiple antennas are discussed.

### A. Effect of the Feeding Structure

An antenna element arranged in the  $xoy$ -plane is used for feeding the Luneburg lens as illustrated in Fig. 6. Three types of antennas, namely an ME-dipole antenna that previously reported in [28], a half-wavelength electric dipole antenna with a resonant frequency at 32 GHz and an open-ended WR-28 waveguide which can be seen as an equivalent magnetic dipole, are considered here to evaluate the influence of the feed on radiation characteristics of the Luneburg lens. The geometry of the ME-dipole antenna is same with that in [28], but its dimensions are magnified two times to guarantee an operating band covering the entire Ka-band. The width of the feeding SIW is 5.7 mm. The distance between the two electric dipoles is 1.7 mm, while the distance between the dipoles and the metallic vertical wall behind the antenna is 3.2 mm. Three Rogers 5880 printed circuit board (PCB) laminates with a thickness of 1.575 mm and a dielectric constant of 2.2 are employed for the antenna design. The spacing  $d$  between the edge of the outermost dielectric ring and the feeding element is 1 mm such that the radiating aperture of the feeding antenna is close to the surface of the gradient-index material.

Simulated electric field distributions across the lens with the three types of feeds are illustrated in Fig. 7. It is seen that the spherical wave from the feed is converted into a planar wave in front of the lens in both the E- and H- planes, which verifies the effectiveness of the proposed design process for the 3D printed Luneburg lens. Because of the omnidirectional radiation features, a strong backward radiation can be observed for the lenses fed by the electric dipole and the open-ended waveguide. Furthermore, the electric field distributions in the two orthogonal planes are not same with each other for the two designs. On the other hand, the backward radiation field can be prevented significantly by utilizing the ME-dipole as the feed

&gt; REPLACE THIS LINE WITH YOUR PAPER IDENTIFICATION NUMBER (DOUBLE-CLICK HERE TO EDIT) &lt;

5

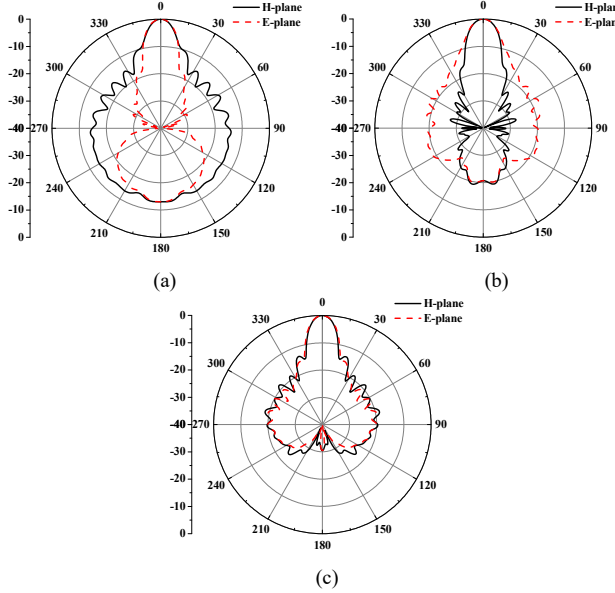


Fig. 8. Simulated radiation patterns of the Luneburg lens with various feed structures. (a) electric dipole, (b) open-ended waveguide, (c) ME-dipole.

TABLE II  
COMPARISON OF THE RADIATION CHARACTERISTICS OF THE 3D-PRINTED  
LUNEBURG LENS WITH DIFFERENT FEEDS

Feed type	3-dB beamwidth in the E-plane	3-dB beamwidth in the H-plane	FTBR (dB)	Gain (dBi)
Electric dipole	13.8°	12.4°	13.1	17.9
Open-ended waveguide	12.4°	13.2°	20.7	19.8
ME-dipole	12.8°	12.4°	30.5	20

as shown in Fig. 7 (c) and (f). The electric field distribution in the E-plane is almost consistent with that in the H-plane, which is contributed to the almost identical radiation patterns of the ME-dipole feed in the two planes.

Simulated radiation patterns of the Luneburg lens fed by the three sorts of antennas are depicted in Fig. 8, where obvious discrepancy between the results can be observed. Detailed values are also summarized in Table II for comparison. Different from unequal radiation patterns in the E- and H-planes realized by using the electric or equivalent magnetic dipole, almost identical radiation patterns in the two orthogonal planes can be achieved when the lens is fed by the ME-dipole. The 3-dB beamwidths in the two planes are almost the same too. Moreover, a large front to back ratio (FTBR) of about 30 dB is obtained by the Luneburg lens. Finally, the use of the ME-dipole feed also leads to a slightly higher gain as shown in Table I. The above discussions demonstrate the superiority of the ME-dipole operating as the feed of the Luneburg lens. Actually, for the multi-beam antenna design, the lens with ME-dipole feeds also has advantages of stable radiation patterns and promising crossover level as will be analyzed in the following sections.

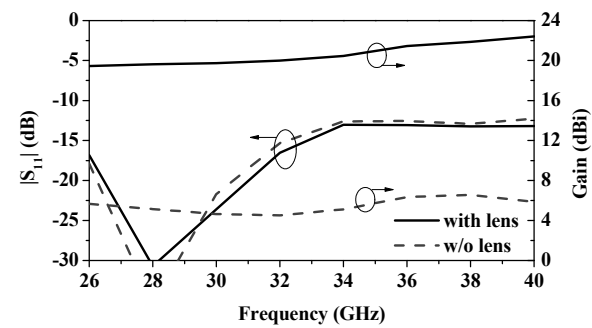


Fig. 9. Simulated  $|S_{11}|$  and gain of the ME-dipole feed with and without the Luneburg lens.

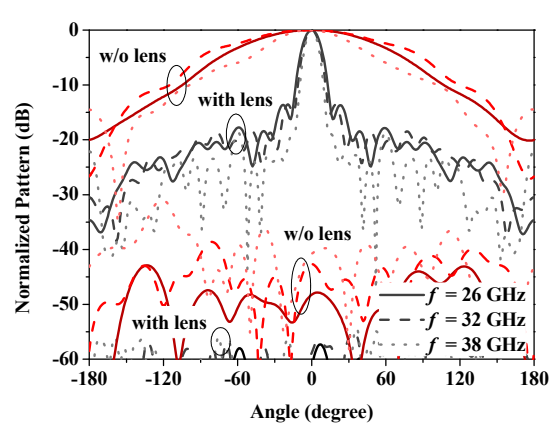
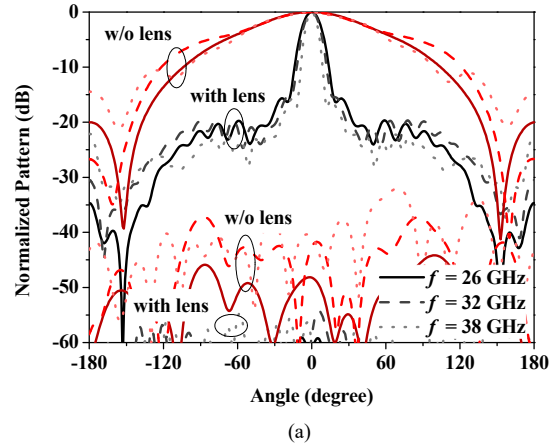


Fig. 10. Simulated radiation patterns of the ME-dipole feed with and without the Luneburg lens. (a) E-plane, (b) H-plane.

### B. Performance of the Lens with an ME-Dipole Feed

Simulated  $|S_{11}|$  and gain of the Luneburg lens with the ME-dipole feed are provided in Fig. 9 accompanied with the performance of the ME-dipole antenna. The existence of the lens does not affect the impedance matching of the feeding antenna significantly and a bandwidth of wider than 42% for  $|S_{11}| < -10$  dB that can cover the entire Ka-band is achieved by the design. On the other hand, the gain varies from 19.5 to 22.4 dBi across the operating band, which is around 14 dB higher than that of the ME-dipole feed.

&gt; REPLACE THIS LINE WITH YOUR PAPER IDENTIFICATION NUMBER (DOUBLE-CLICK HERE TO EDIT) &lt;

6

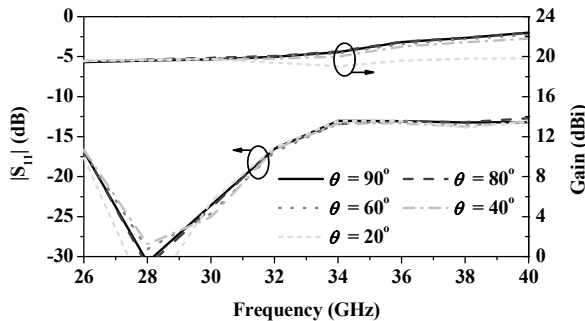


Fig. 11. Simulated  $|S_{11}|$  and gain of the Luneburg lens antenna with an ME-dipole feed located at different elevated angles  $\theta$ .

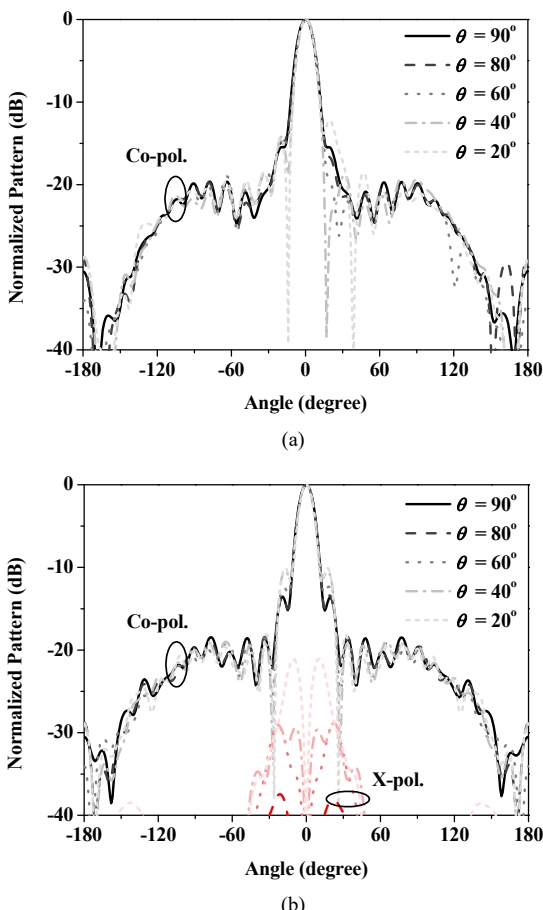


Fig. 12. Simulated radiation pattern of the Luneburg lens antenna with an ME-dipole feed located at different elevated angles  $\theta$ . (a) E-plane, (b) H-plane.

Fig. 10 presents the simulated radiation patterns of the lens antenna at different frequencies. The radiation patterns are stable in the E- and H- planes throughout the operating band because of desirable radiation features of the ME-dipole feed, while the beamwidth is gradually decreased with the increase of frequency. In addition, the cross polarization level is almost less than -35 dB at different frequencies.

In order to realize the multi-beam radiation, several feeding antennas should be arranged simultaneously at the edge of the lens. Considering that the proposed 3D printed Luneburg lens is constructed by the anisotropic gradient-index material, its

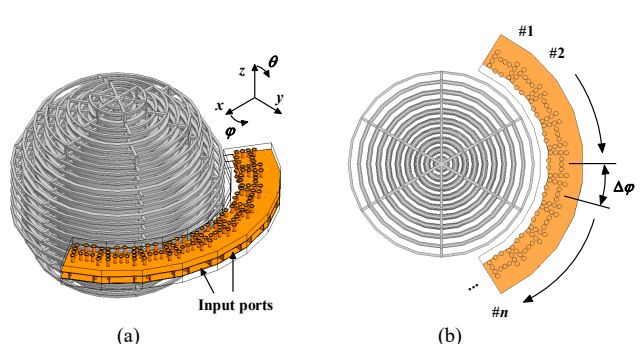


Fig. 13. Geometry of the multi-beam Luneburg lens antenna with multiple ME-dipole feeds. (a) Perspective view, (b) top view.

performance for a feeding antenna at different locations is then analyzed to guarantee stable beam-scanning features of the multi-beam antenna. Due to the rotational symmetry of the lens geometry, the beam scanning feature does not change with the azimuth angle  $\phi$  as illustrated in Fig. 7. Therefore, only the scanning feature in the elevation plane is investigated. As shown in Fig. 11, the impedance matching of the feeding antenna is not affected by the elevated angle  $\theta$ . The gain of the lens antenna almost stays the same for  $\theta$  varying from  $90^\circ$  to  $40^\circ$ . Slightly decrease can be observed when  $\theta = 20^\circ$ , but the gain is still higher than 19 dBi throughout the operating band. Furthermore, Fig. 12 presents the simulated radiation patterns for various  $\theta$ , in which the radiation pattern is stable in the E-plane and the cross polarization is less than -40 dB. The first sidelobe level and the cross polarization in the H-plane gradually increase for  $\theta$  varying from  $90^\circ$  to  $20^\circ$ . However, the shape of the main beam is not changed significantly with  $\theta$ , and the sidelobe and cross polarization level are still satisfactory in comparison with the conventional multi-beam antennas. Actually, with the decrease of  $\theta$ , the polarization of an increasing portion of the wave from the feeding antenna will be parallel to the dielectric rings, which is same with the case of horizontal polarization discussed in Section II. Therefore, the effective dielectric constant of the gradient-index material is changed, and thus the radiation feature of the lens antenna is degraded. As a conclusion, promising scanning performance can be achieved by the proposed 3D-printed Luneburg lens antenna within an angular range of  $\pm 70^\circ$  in the elevation plane and  $360^\circ$  in the azimuth plane, which would be wide enough for most application scenarios in wireless communications.

### C. Multi-Beam Luneburg Lens Antenna

Based on the investigations above, the multi-beam Luneburg lens antenna is designed in this section. A set of the ME-dipole antennas is assigned in the xoy-plane as the feed of the lens antenna as illustrated in Fig. 13. Benefiting from the utilization of the ME-dipole antennas with end-fire radiation, the feeding structure can be arranged at the edge of the planar PCB substrates conveniently and a small volume is occupied. Rest portions of the communication system including the RF chains and digital circuits can be integrated into the area behind the antennas as indicated in [4] and [5]. Hence, the whole system would have a compact structure in practice.

&gt; REPLACE THIS LINE WITH YOUR PAPER IDENTIFICATION NUMBER (DOUBLE-CLICK HERE TO EDIT) &lt;

7

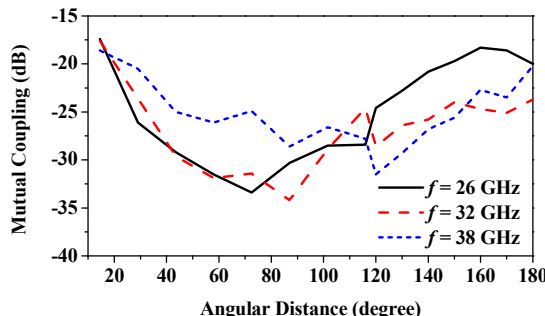


Fig. 14. Simulated mutual coupling between two ME-dipole feeds with different angular distances.

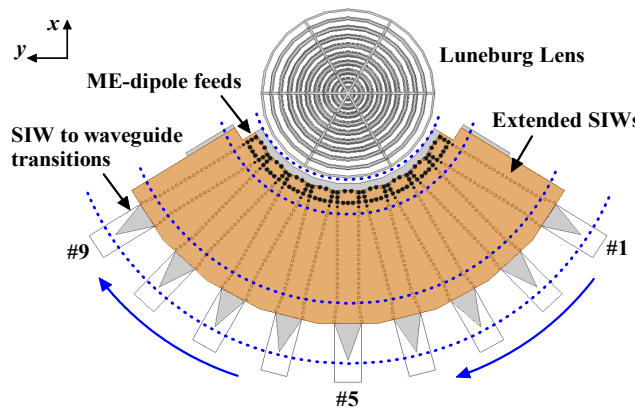


Fig. 15. Geometry of the proposed 3D printed multi-beam Luneburg lens fed by ME-dipoles.

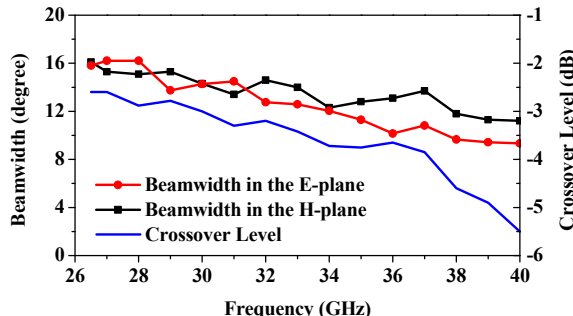


Fig. 16. Simulated beamwidths of the radiation beam and the crossover level between neighboring beams.

Simulated mutual coupling between two feeding antennas with a varying angular distance is exhibited in Fig. 14. The minimum angular distance between the adjacent feeds depends on the width of the ME-dipole antenna and is about 14.5° in this design. It is seen in Fig. 14 that the mutual coupling gradually reduces when the angular distance increases from 14.5° to 90°. After that, it increases again with the angular distance because of opposite radiating directions of the two antennas. The mutual coupling is below -17 dB over the Ka-band for various angular distances.

The overall configuration of the multi-beam 3D printed Luneburg lens antenna with nine feeding elements is proposed in Fig. 15. The angular distance between the feeding antennas is set to 14.5°. The input ports of the feeding ME-dipoles are

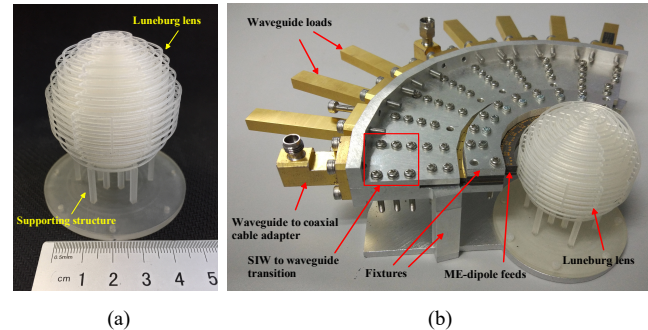


Fig. 17. Photographs of the fabricated prototype of the proposed multi-beam 3D printed Luneburg lens antenna fed by ME-dipoles. (a) 3D printed Luneburg lens, (b) multi-beam antenna connecting with adapters and waveguide loads.

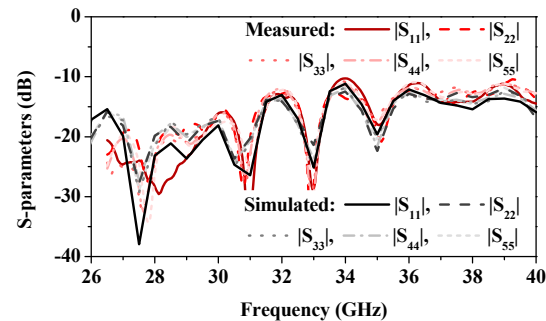


Fig. 18. Measured and simulated reflection coefficient of the multi-beam Luneburg lens antenna.

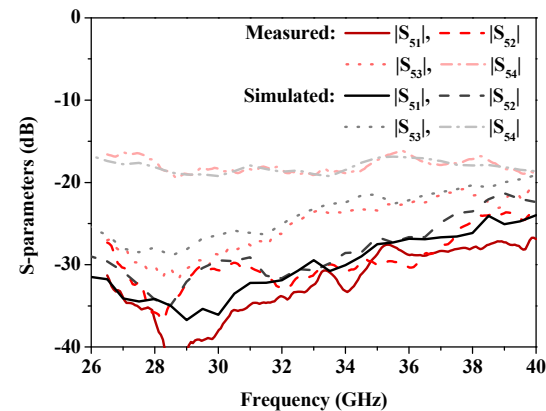


Fig. 19. Measured and simulated mutual coupling of the multi-beam Luneburg lens antenna.

extended outward for convenience of measurement. The SIW to air-filled rectangular waveguide transitions reported in [31] are applied as well. Fig. 16 provides the beamwidths in the E- and H- planes and the crossover level between two neighboring beams. It is noted that because the characteristics of the beams are quite similar to each other, only the results when Port 5 is excited is shown in Fig. 16 for simplification. It is observed that the difference between the 3-dB beamwidths in the two orthogonal planes is smaller than 3° throughout the operating band. Moreover, due to the reduction of the beamwidth, the crossover level decreases from -2.6 dB at 26.5 GHz to -5.5 dB at 40 GHz.

> REPLACE THIS LINE WITH YOUR PAPER IDENTIFICATION NUMBER (DOUBLE-CLICK HERE TO EDIT) <

8

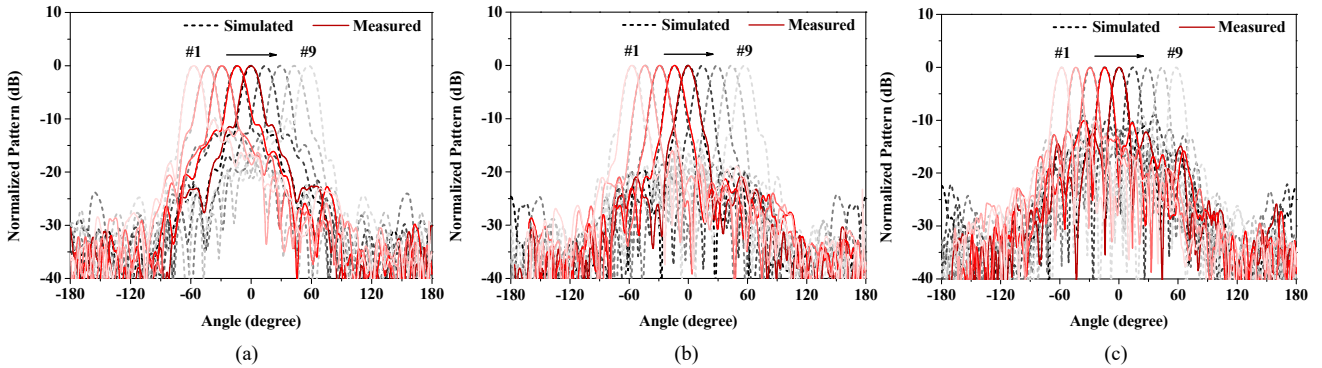


Fig. 20. Measured and simulated radiation patterns of the multi-beam Luneburg lens antenna. (a)  $f = 26.5$  GHz, (b)  $f = 32$  GHz, (c)  $f = 38$  GHz.

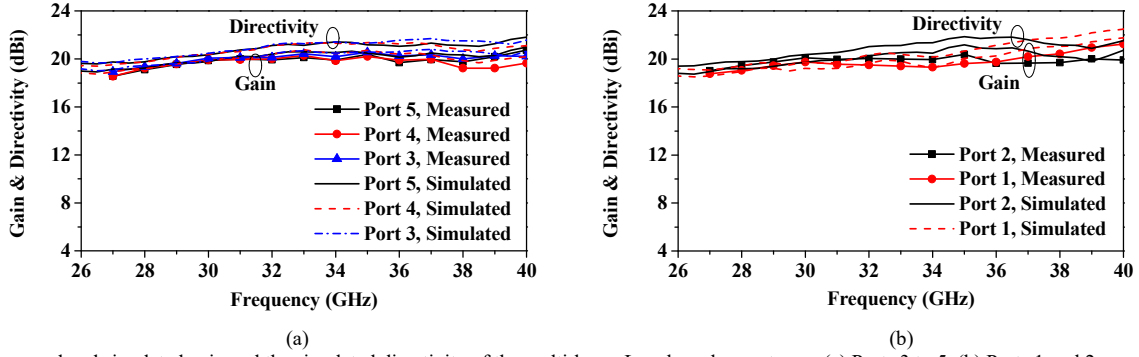


Fig. 21. Measured and simulated gain and the simulated directivity of the multi-beam Luneburg lens antenna. (a) Ports 3 to 5, (b) Ports 1 and 2.

TABLE III  
COMPARISON BETWEEN PROPOSED AND REPORTED LUNEBURG LENS ANTENNAS

Ref.	Lens realization	Feed Type	$f_0$ (GHz)	BW (-10 dB)	Gain (dBi)	No. of beams	Antenna efficiency	Crossover level (dB)
[23]	n.a.	$2 \times 2$ patch array	15	13%	30.7-31.3	1	n.a.	n.a.
[16]	Perforated slices	Open-ended waveguide	15	58%	24.3-25.7	1	57%-86%	n.a.
[15]	Perforated slices	Open-ended waveguide	33	40%	22.5-28.5	1	22%-50%	n.a.
[24]	Perforated and pressed slices	Planar log periodic dipole	80	9.3%	10.1-15.4	17	n.a.	-4 to -5
[20]	3D printing (cubical lattices)	Open-ended waveguide	33	30%	19-26	1	n.a.	n.a.
[21]	3D printing (cubical lattices)	Open-ended waveguide	10	40%	17.3-20.3	1	40%-50%	n.a.
This work	3D printing (dielectric rings)	ME-dipole	33	40%	18.6-21.2	9	35%-49%	-2.6 to -5.5

#### IV. MEASUREMENT AND DISCUSSION

The proposed multi-beam 3D printed Luneburg lens antenna fed by ME-dipoles was manufactured and measured to verify the design. The 3D printed Luneburg lens prototype is exhibited in Fig. 17 (a), where a supporting structure has been added to maintain the position of the lens. Three aluminium fixtures with location pins and screws were utilized for antenna assembly and alignment as indicated in Fig. 17 (b). During S-parameter measurement, two of the input ports were connected with waveguide to coaxial cable adapters, while the others were terminated with waveguide loads. Only one port

was excited at one time for testing the radiating performance. An Agilent Network Analyzer E8363C and a far-field anechoic chamber were employed to perform the input port features and radiating characteristics, respectively. The gain of the antenna was obtained by comparing with standard gain horns.

##### A. S-parameter

Measured and simulated reflection coefficients of Ports 1 to 5 are in good agreement as given in Fig. 18. The measured overlapped impedance bandwidth for the reflection coefficient of less than -10 dB is wider than 40%, which can cover the entire Ka-band. Due to the symmetrical geometry of the

&gt; REPLACE THIS LINE WITH YOUR PAPER IDENTIFICATION NUMBER (DOUBLE-CLICK HERE TO EDIT) &lt;

9

proposed multi-beam lens antenna, results of Ports 6 to 9 are similar to the counterparts of Ports 1 to 4. On the other hand, it is seen in Fig. 19 that the measured mutual couplings between Port 5 and the other eight ports also agrees well with the simulated one. Same with the simulated results discussed in Section V-C, the measured mutual coupling between the two adjacent ports, i.e. Ports 4 and 5, is the highest, which is lower than -17 dB throughout the operating band. Additionally, measured  $|S_{51}|$  to  $|S_{53}|$  are less than -20 dB.

### B. Radiation Pattern

Fig. 20 provides the measured and simulated radiation patterns of the multi-beam antenna scanning in the horizontal plane at 26.5, 32 and 38 GHz, respectively, in which the red solid lines indicate the measured results and the black dash lines indicate the simulation. The radiation performance is almost identical when the input ports are excited separately. The nine radiating beams can cover an angular range between  $\pm 61^\circ$ . The simulated cross polarization of less than -25 dB is omitted for the purpose of simplification. Besides, the measured results are not easy to obtain accurately due to the limited transmitting power in the laboratory.

### C. Gain and Efficiency

Fig. 21 illustrates the measured and simulated gain of the antenna and the simulated directivity when Ports 1 to 5 are excited separately. The insertion loss caused by the waveguide to SIW transition and the waveguide to coaxial cable adapter has been calibrated. The measured gain curves for different ports are not changed significantly and consistent well with the simulated results. Measured gain up to 21.2 dBi is achieved and the variation of the gain is less than 2.5 dB over the operating band, which means that the 3-dB gain bandwidth can cover the Ka-band as well.

By comparing the measured gain with the simulated directivity, the estimated radiation efficiency of the fabricated prototype is around 75%. As there is no complex feed network in this design, the gain decrease in comparison with the directivity can be mainly attributed to the dielectric loss of the 3D printing material.

### D. Comparison and discussion

The effectiveness of the proposed multi-beam antenna has been demonstrated by the experimental results. In order to better evaluate the characteristics of the design, a comparison between the Luneburg lens antennas reported in the literature and this work is summarized in Table III. In terms of the feeding structure, the open-ended waveguide is employed by most reported Luneburg lens designs with wide bandwidths, but only single radiation beam is accomplished due to the low integration level of the waveguide feed [15], [16], [20], [21]. Constrained by the characteristics of the planar feeding antennas, the bandwidth of the Luneburg lens is only around 10%, which is not promising for wideband mm-wave wireless applications [23], [24]. With the help of the ME-dipole antennas, the operating bandwidth of 40% and stable multi-beam radiation performance can be achieved in this work. Moreover, the crossover level of the design is relatively low because of the compact geometry of the SIW fed ME-dipole. It

is noted that improved crossover level feature at the high end of the operating band would be achieved in practice if substrates with a higher dielectric constant are utilized for the feed element design.

In comparison with other mm-wave Luneburg lenses constructed by gradient-index materials [15], [20], [24], the gain with a small variation is realized across a wide operating band in this work, which can be mainly attributed to the use of the rod-type material with a wider tuning range in the effective dielectric constant at mm-waves. Besides, the antenna efficiency of this design is comparable with the counterpart of the designs in lower operating frequencies [16], [21].

## V. CONCLUSION

A multi-beam 3D printed Luneburg lens antenna with a novel configuration has been proposed in Ka-band. With the employment of the rod-type gradient-index material, the lens structure can be fabricated successfully by the commercial 3D printing technique. Substrate integrated waveguide fed magneto-electric dipoles with end-fire radiation have been introduced as the feed of the Luneburg lens, which makes the radiation characteristics stable over a wide operating band and the geometry of the entire design compact. The presented multi-beam antenna design with low costs is valuable to the millimeter-wave multiple-input multiple-output applications in the fifth-generation mobile communications.

## REFERENCES

- [1] T. S. Rappaport et al., *Millimeter Wave Wireless Communications*, Prentice Hall, 2014.
- [2] A. Alkhateeb, J. Mo, N. González-Prelcic, and R. W. Heath, "MIMO precoding and combining solutions for millimeter-wave systems," *IEEE Commun. Mag.*, vol. 52, no. 12, pp. 122–131, Dec. 2014.
- [3] S. Han, C.-L. I, Z. Xu, and C. Rowell, "Large-scale antenna systems with hybrid precoding analog and digital beamforming for millimeter wave 5G," *IEEE Commun. Mag.*, vol. 53, no. 1, pp. 186–194, Jan. 2015.
- [4] J. Brady, N. Behdad, and A. M. Sayeed, "Beamspace MIMO for Millimeter-Wave Communications: System Architecture, Modeling, Analysis, and Measurements," *IEEE Trans. Antennas Propag.*, vol. 61, no. 7, July 2013, pp. 3814–27.
- [5] X. Gao, L. Dai, S. Han, C.-L. I, and X. Wang, "Reliable beamspace channel estimation for millimeter-wave massive MIMO systems with lens antenna array," *IEEE Trans. Wireless Commun.*, vol. 16, no. 9, pp. 6010–6021, Sep. 2017.
- [6] J. Ala-Laurinaho et al., "2-D beam-steerable integrated lens antenna system for 5G E-band access and backhaul," *IEEE Trans. Microw. Theory Techn.*, vol. 64, no. 7, pp. 2244–2255, Jul. 2016.
- [7] Marc Imbert et al., "Assessment of LTCC-Based Dielectric Flat Lens Antennas and Switched-Beam Arrays for Future 5G Millimeter-Wave Communication Systems," *IEEE Trans. Antennas Propag.*, vol. 65, no. 12, pp. 6453–6473, Dec. 2017.
- [8] B. Schoenlinner, X. Wu, J. P. Ebling, G. V. Eleftheriades, and G. M. Rebeiz, "Wide-scan spherical-lens antennas for automotive radars," *IEEE Trans. Microwave Theory Tech.*, vol. 50, no. 9, pp. 2166–2175, Sep. 2002.
- [9] Z. Briqech, "Wide-Scan MSC-AFTSA Array-Fed Grooved Spherical Lens Antenna for Millimeter-Wave MIMO Applications," *IEEE Trans. Antennas Propag.*, vol. 64, no. 7, pp. 2971–2980, Jul. 2016.
- [10] R. K. Luneburg, *The Mathematical Theory of Optics*. Providence. R. I.: Brown University Press, 1944. (Reprint. Berkeley, Calif.: University of California Press. 1964.)
- [11] John Thornton and Kao-Cheng Huang, *Modern Lens Antennas for Communications Engineering*, Wiley-IEEE Press, Apr. 2013.

&gt; REPLACE THIS LINE WITH YOUR PAPER IDENTIFICATION NUMBER (DOUBLE-CLICK HERE TO EDIT) &lt;

10

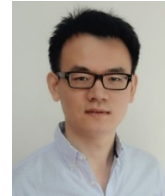
- [12] H. Mosallaei and Y. Rahmat-Samii, "Nonuniform luneburg and two-shell lens antennas: Radiation characteristics and design optimization," *IEEE Trans. Antennas Propag.*, vol. 49, no. 1, pp. 60–69, Jan. 2001.
- [13] B. Fuchs, L. L. Coq, O. Lafond, S. Rondineau, and M. Himdi, "Design optimization of multishell luneburg lenses," *IEEE Trans. Antennas Propag.*, vol. 55, no. 2, pp. 283–289, Feb. 2007.
- [14] A. V. Boriskin, A. Vorobyov, and R. Sauleau, "Two-shell radially symmetric dielectric lenses as low-cost analogs of the Luneburg lens," *IEEE Trans. Antennas Propag.*, vol. 59, no. 8, pp. 3089–3093, Aug. 2011.
- [15] S. Rondineau, M. Himdi, and J. Sorieux, "A sliced spherical Lüneburg lens," *IEEE Antennas Wireless Propag. Lett.*, vol. 2, pp. 163–166, 2003.
- [16] H. F. Ma, B. G. Cai, T. X. Zhang, Y. Yang, W. X. Jiang, and T. J. Cui, "Three-dimensional gradient-index materials and their applications in microwave lens antennas," *IEEE Trans. Antennas Propag.*, vol. 61, no. 5, pp. 2561–9, May 2013.
- [17] H. Xin, and M. Liang, "3-D-Printed Microwave and THz Devices Using Polymer Jetting Techniques," *Proceedings of the IEEE*, vol. 105, no. 4, pp. 737–755, Apr. 2017.
- [18] H. Yi, S.-W. Qu, K.-B. Ng, C. H. Chan, and X. Bai, "3-D printed millimeter-wave and terahertz lenses with fixed and frequency scanned beam," *IEEE Trans. Antennas Propag.*, vol. 64, no. 2, pp. 442–449, Feb. 2016.
- [19] K. X. Wang and H. Wong, "A wideband millimeter-wave circularly polarized antenna with 3-D printed polarizer," *IEEE Trans. Antennas Propag.*, vol. 65, no. 3, pp. 1038–1046, Mar. 2017.
- [20] K. Brakora, J. Halloran, and K. Sarabandi, "Design of 3-D monolithic MMW antennas using ceramic stereolithography," *IEEE Trans. Antennas Propag.*, vol. 55, no. 3, pp. 790–797, Mar. 2007.
- [21] M. Liang, W. R. Ng, K. Chang, K. Gbele, M. E. Gehm, and H. Xin, "A 3-D Luneburg lens antenna fabricated by polymer jetting rapid prototyping," *IEEE Trans. Antennas Propag.*, vol. 62, no. 4, pp. 1799–1807, Apr. 2014.
- [22] M. Ignatenko et al., "A Phase Center-Stabilized K/Ka/V-Band Linearly Polarized Horn for Luneburg Lenses," *IEEE Antennas Wireless Propag. Lett.*, vol. 16, pp. 2726–2729, 2017.
- [23] A. R. Weily and N. Nikolic, "Dual-Polarized Planar Feed for Low-Profil le Hemispherical Luneburg Lens Antenna," *IEEE Transactions on Antennas and Propagation*, vol. 60, no. 1, pp. 402–407, Jan. 2012.
- [24] M. K. Saleem et al., "Lens Antenna for Wide Angle Beam Scanning at 79 GHz for Automotive Short Range Radar Applications," *IEEE Trans. Antennas Propag.*, vol. 65, no. 4, pp. 2041–2046, Apr. 2017.
- [25] K.-M. Luk and H. Wong, "A new wideband unidirectional antenna element," *Int. J. Microw. Opt. Technol.*, vol. 1, no. 1, pp. 35–44, Jun. 2006.
- [26] K. B. Ng, H. Wong, K. K. So, C. H. Chan, and K. M. Luk, "60 GHz plated through hole printed magneto-electric dipole antenna," *IEEE Trans. Antennas Propag.*, vol. 60, no. 7, pp. 3129–3136, Jul. 2012.
- [27] Yujian Li and Kwai-Man Luk, "60-GHz dual-polarized two-dimensional switch-beam wideband antenna array of aperture-coupled magneto-electric dipoles," *IEEE Trans. Antennas Propag.*, vol. 64, no. 2, pp. 554–563, Feb. 2016.
- [28] Yujian Li and Kwai-Man Luk, "A multibeam end-fire magnetoelectric dipole antenna array for millimeter-wave applications," *IEEE Trans. Antennas Propag.*, vol. 64, no. 7, pp. 2894–2904, Jul. 2016.
- [29] Ansoft Corp., Canonsburg, PA, USA. HFSS: High Frequency Structure Simulator Based on the Finite Element Method. [Online]. Available: <http://www.ansoft.com/>
- [30] X. Chen et al., "Robust method to retrieve the constitutive effective parameters of metamaterials," *Physical Review E*, Jul. 2004.
- [31] D. Dousset, K. Wu, and S. Claude, "Millimeter-wave broadband transition of substrate-integrated waveguide to rectangular waveguide," *Electron. Lett.*, vol. 46, no. 24, pp. 1610–1611, Nov. 2010.



**Yujian Li** (S'12–M'15) was born in Hunan, China, in 1987. He received the B.S. and M.S. degrees in communications engineering from Beijing Jiaotong University, Beijing, China, in 2009 and 2012, respectively, and the Ph.D. degree in electronic engineering from City University of Hong Kong in 2015.

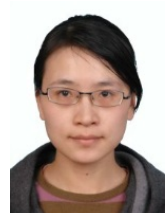
He joined the Institute of Lightwave Technology at Beijing Jiaotong University in 2015 as an Associate Professor. His current research interests include millimeter wave antennas, base station antennas and leaky wave structures.

Dr. Li was awarded the Outstanding Research Thesis Award from City University of Hong Kong in 2015. He received the Best Paper Award at the 2015 IEEE Asia-Pacific Conference on Antennas and Propagation (APCAP), the Best Student Paper at 2013 National Conference on Antennas, and the Best Student Paper Award (2<sup>nd</sup> Prize) at the 2013 IEEE International Workshop on Electromagnetics (iWEM). He was selected as a Finalist in the student paper contest of 2015 IEEE AP-S Symposium on Antennas and Propagation (APS). He has served as a Reviewer for the IEEE Transactions on Antennas and Propagation, the IEEE Antennas and Wireless Propagation Letters, and the IET Microwaves, Antennas & Propagation.



**Lei Ge** (S'11–M'15) was born in Jiangsu, China. He received the B.S. degree in electronic engineering from Nanjing University of Science and Technology, Nanjing, China, in 2009 and the Ph.D. degree in electronic engineering from City University of Hong Kong, Hong Kong, in 2015. From September 2010 to July 2011, he was a Research Assistant with the City University of Hong Kong. From April 2015 to October 2015, he was a Postdoctoral Research Fellow at the State Key Laboratory of Millimeter Waves, City University of Hong Kong. He is currently Assistant Professor and Associate Head of Department of Electronic Engineering at Shenzhen University, China.

He received the Honorable Mention at the student contest of 2012 IEEE APS-URSI Conference and Exhibition held in Chicago, US. He won the 1<sup>st</sup> Prize in the Student Innovation Competition of 2014 IEEE International Workshop on Electromagnetics (IEEE iWEM) held in Sapporo, Japan, in 2014. He was the Session Chair of the iWEM 2017 and ACES-China 2017. He was the TPC Member of the APCAP 2016. His recent research interest focuses on wideband antennas, patch antennas, base station antennas, reconfigurable antennas, the antennas for cognitive radio, and filtering antennas.



**Meie Chen** received the B.S. degree in Information and Tele-communication Engineering and Ph.D. degree in Electromagnetic and Microwave Technology from Beijing Jiaotong University, Beijing, China, in 2003 and 2009, respectively.

She is currently a lecture in the Institute of Lightwave Technology at Beijing Jiaotong University. Her research interests include antenna theory and technology, metasurface, RCS reduction technique.



**Zhan Zhang** received B.S. degree in Electronics and Communications Engineering from Jilin University, China in 2002 and Ph.D. degree in electrical engineering from Nanyang Technological University, Singapore, in 2010. She joined the Faculty of School of Electronics and Information Engineering, Beijing Jiaotong University, Beijing, China, in 2010, where she is currently an associate professor. Her current research interests include metamaterial-based antenna design and transformation optics.



**Zheng Li** received the B.S. degree in physics and M.S. degree in electrical engineering from Beijing Jiaotong University, Beijing, China, in 2006 and 2012, respectively. From 2008 to 2009, he was a visiting student with the Pennsylvania State University, Pennsylvania, USA.

In 2012, he joined the faculty of the Department of Electrical Engineering, Beijing Jiaotong University, where he became an associate professor in 2015. His research interests include leaky-wave antennas and periodic structures.



**Junhong Wang** (M'02–SM'03) was born in Jiangsu, China, in 1965. He received the B.S. and M.S. degrees in electrical engineering from the University of Electronic Science and Technology of China, Chengdu, China, in 1988 and 1991, respectively, and the Ph.D. degree in electrical engineering from Southwest Jiaotong University, Chengdu, China, in 1994. In 1995, he joined as the Faculty with the Department of Electrical Engineering,

> REPLACE THIS LINE WITH YOUR PAPER IDENTIFICATION NUMBER (DOUBLE-CLICK HERE TO EDIT) < 11

Beijing Jiaotong University, Beijing, China, where he became a Professor in 1999. From January 1999 to June 2000, he was a Research Associate with the Department of Electric Engineering, City University of Hong Kong, Kowloon Tong, Hong Kong. From July 2002 to July 2003, he was a Research Scientist with Temasek Laboratories, National University of Singapore, Singapore. He is currently with the Key Laboratory of all Optical Network and Advanced Telecommunication Network, Ministry of Education of China, Beijing Jiaotong University, Beijing, China, and also with the Institute of Lightwave Technology, Beijing Jiaotong University, Beijing, China. His research interests include numerical methods, antennas, scattering, and leaky wave structures.